Cyanide-Bridged Lanthanide(III)−Transition Metal Extended Arrays: Interconversion of One-Dimensional Arrays from Single-Strand (Type A) to Double-Strand (Type B) Structures. Complexes of a New Type of Single-Strand Array (Type C)

Jianping Liu, David W. Knoeppel, Shengming Liu, Edward A. Meyers, and Sheldon G. Shore*

Department of Chemistry, The Ohio State University, Columbus, Ohio 43210

Received October 17, 2000

A series of one-dimensional arrays of lanthanide−transition metal complexes has been prepared and characterized. These complexes, $\{(DMF)_{10}Ln_2[Ni(CN)_4]_3\}_\infty$, crystallize as linear single-strand arrays (structural type A) (Ln = Sm, **1a**; Eu, **2a**) or double-strand arrays (structural type B) (Ln = Sm, **1b**; Eu, **2b**) depending upon the conditions chosen, and they are interconvertible. The single-strand type A structure can be converted to the double-strand type B structure. When the **1b** and **2b** type B crystals are completely dissolved in DMF, their infrared spectra are identical to the infrared spectra of **1a** and **2a** type A crystals dissolved in DMF. These solutions produce type A crystals initially. It is believed that formation of the type A structure is kinetically favored while the type B structure is thermodynamically favored for lanthanide−nickel complexes **1** and **2**. On the other hand the complex $\{(DMF)_{10}Y_2[Pd(CN)_4]_3\}_\infty$, **3**, appears to crystallize only as the double-strand array (type B**)**. The complexes $\{(DMF)_{12}Ce_2[Ni(CN)_4]_3\}_\infty$, **4**, and $\{(DMF)_{12}Ce_2[Pd(CN)_4]_3\}_\infty$, **5,** crystallize as a new type of single-strand array (structural type C). This structural type is a zigzag chain array. Crystal data for **1a**: triclinic space group $P\bar{1}$, $a = 10.442(5)$ Å, $b = 10.923(2)$ Å, $c = 15.168(3)$ Å, $\alpha = 74.02(2)°$, $\beta = 83.81(3)°$, $\gamma = 82.91(4)°$, $Z = 2$. Crystal data for **1b**: triclinic space group $P\bar{1}$, $a = 9.129(2)$ Å, $b = 11.286(6)$ Å, $c = 16.276(7)$ Å, $\alpha = 81.40(4)°$, $\beta = 77.41(3)°$, $\gamma = 83.02(3)°$, $Z = 2$. Crystal data for **2a**: triclinic space group $P\bar{1}$, $a = 10.467(1)$ Å, $b = 10.923(1)$ Å, $c = 15.123(1)$ Å, $\alpha = 74.24(1)°$, $\beta = 83.61(1)°$, $\gamma = 83.13(1)°$, $Z = 2$. Crystal data for **2b**: triclinic space group $P\bar{1}$, $a = 9.128(1)$ Å, $b = 11.271(1)$ Å, $c = 16.227(6)$ Å, $\alpha = 81.36(2)°$, $\beta = 77.43(2)°$, $\gamma = 82.99(1)°$, $Z = 2$. Crystal data for **3**: triclinic space group $P\bar{1}$, $a = 9.251(3)$ Å, $b = 11.193(4)$ Å, $c = 16.388(4)$ Å, $\alpha = 81.46(2)°$, $\beta = 77.18(2)°$, $\gamma = 83.24(3)°$, $Z = 2$. Crystal data for **4**: triclinic space group $P\bar{1}$, $a = 11.279(1)$ Å, $b = 12.504(1)$ Å, $c = 13.887(1)$ Å, $\alpha = 98.68(1)°$, $\beta = 108.85(1)°$, $\gamma = 101.75(1)°$, $Z = 2$. Crystal data for **5**: triclinic space group $P\bar{1}$, $a = 11.388(3)$ Å, $b = 12.614(5)$ Å, $c = 13.965(4)$ Å, $\alpha = 97.67(3)°$, $\beta = 109.01(2)°$, $\gamma = 101.93(2)°$, $Z = 2$.

Introduction

Heterometallic complexes that contain both lanthanide and transition metals bridged by cyanide ligand are of interest because they can be employed as precursors in the preparation of various materials, such as rare earth orthoferrites (perovskite-type oxides),[1] electroceramic[2] and chemical sensor materials,[3] and fluorescent materials.[4] Lanthanides in combination with transition metals have been shown to have a positive effect in promoting heterogeneous catalytic reactions.[5] Cyanide-bridged lanthanide−transition metal arrays offer the potential advantage of simultaneously loading both types of metals onto a surface in an intimate fashion, in a simpler and easier manner than a more conventional technique of separate impregnation of the two metals on the support surface. We have recently shown that the bimetallic Yb−Pd catalyst obtained from the precursor $\{(DMF)_{10}Yb_2[Pd(CN)_4]_3\}_\infty$ on a titania surface offers improved performance over palladium-only catalyst for the reduction of NO by CH_4 in the presence of O_2.[6]

In our general studies of cyanide-bridged lanthanide−transition metal complexes, we are interested in determining and categorizing the types of solid state extended arrays that form and the factors that determine the type of array formed. Earlier we reported syntheses of the one-dimensional arrays, $\{(DMF)_{10}Ln_2[M(CN)_4]_3\}_\infty$ (Ln = Sm, Eu, Er, Yb and M = Ni, Pd, Pt), in reactions of 2:3 molar ratios of $LnCl_3$ and $K_2[M(CN)_4]$ in DMF.[7] Single-crystal X-ray diffraction analyses showed that these complexes possess the general formula

(1) (a) Gallagher, P. K. *Mater. Res. Bull.* **1968**, *3*, 225. (b) Sadaoka, Y.; Aono, H.; Traversa, E.; Sakamoto, M. *J. Alloys Compd.* **1998**, *278*, 135 and references therein.

(2) (a) Shuk, P.; Vecher, A.; Kharton, V.; Tichonova, L.; Wiemhöfer, H. D.; Guth, U.; Göpel, W. *Sens. Actuators, B* **1993**, *16*, 401. (b) Sadaoka, Y.; Traversa, E.; Sakamoto, M. *J. Mater. Chem.* **1996**, *6* (8), 1355.

(3) (a) Matuura, Y.; Matsushima, S.; Sakamoto, M.; Sadaoka, Y. *J. Mater. Chem.* **1993**, *3* (7), 767. (b) Traversa, E.; Matsushima, S.; Okada, G.; Sadaoka, Y.; Sakai, Y.; Watanabe, K. *Sens. Actuators, B* **1995**, *25*, 661.

(4) Sakamoto, M.; Matsuki, K.; Ohsumi R.; Nakayama, Y.; Matsumoto, A.; Okawa, Y. *Bull. Chem. Soc. Jpn.* **1992**, *65*, 2278.

(5) (a) Imamura, H.; Miura, Y.; Fujita, K.; Sakata, Y.; Tsuchiya, S. *J. Mol. Catal. A* **1999**, *140*, 81. (b) Imamura, H.; Igawa, K.; Sakata, Y.; Tsuchiya, S. *Bull. Chem. Soc. Jpn.* **1996**, *69*, 325. (c) Imamura, H.; Igawa, K.; Kasuga, Y.; Sakata, Y.; Tsuchiya, S. *J. Chem. Soc., Faraday Trans.* **1994**, *90*, 2119.

(6) Rath, A.; Liu, J.; Shore, S. G.; Aceves, E.; Mitome, J.; Ozkan, U. S. *J. Mol. Catal. A: Chem.* **2001**, *165*, 103.

(7) (a) Knoeppel, D. W.; Liu, J.; Meyers, E. A.; Shore, S. G. *Inorg. Chem.* **1998**, *37*, 4828. (b) Knoeppel, D. W.; Shore, S. G. *Inorg. Chem.* **1996**, *35*, 1747.

10.1021/ic001143p CCC: $20.00
Published on Web 05/05/2001

Scheme 1

1. Formation of repeating unit

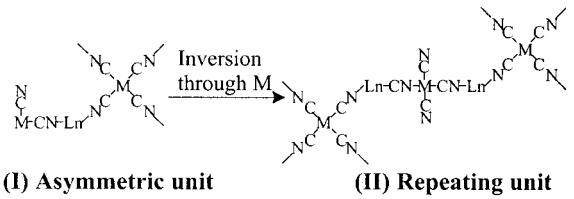

2. Formation of type **A** complexes.

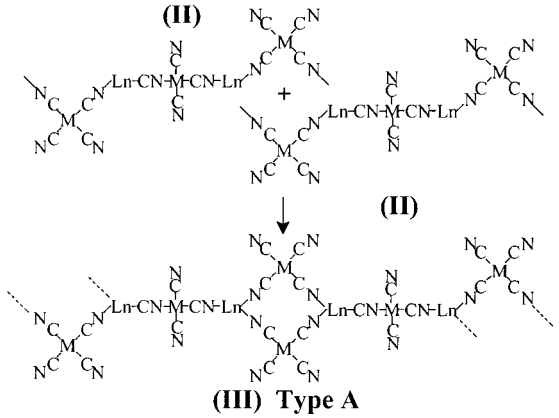

3. Formation of type **B** complexes.

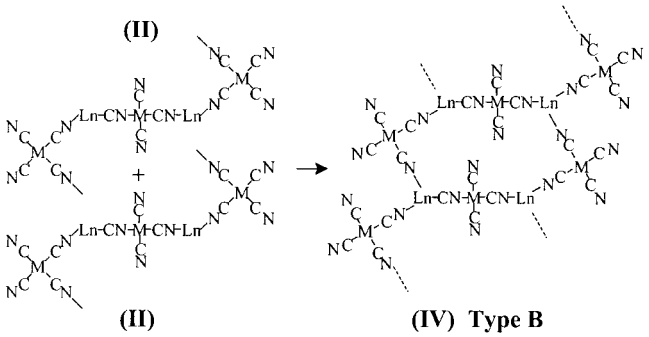

$\{(DMF)_{10}Ln_2[M(CN)_4]_3\}_\infty$ with two different, yet related, one-dimensional structures, designated as structural types A (a single-strand structure) and B (a double-strand structure). Both structural types have the same asymmetric unit $\{[M(CN)_2]Ln(DMF)_5[M(CN)_4]\}$ (**I** in Scheme 1) and the same repeating unit $\{[M(CN)_4](DMF)_5Ln[M(CN)_4]Ln(DMF)_5[M(CN)_4]\}$ (**II** in Scheme 1). The difference between the type A and B structures arises from the combination of the repeating units in the arrays as shown in Scheme 1.[7] Arrays of structural type A (**III** in Scheme 1) consist of a single-strand chain in which *cis*-cyanide-bridged "diamond"-shaped Ln_2Ni_2 metal cores are linked together through *trans*-cyanide-bridging $[Ni(CN)_4]^{2-}$ anions. Arrays with structural type B (**IV** in Scheme 1) consist of two inverted parallel zigzag chains that are connected through the lanthanide atoms by trans-bridging $[M(CN)_4]^{2-}$ (M = Ni, Pd, Pt) anions.

Here, we provide examples of complexes with the type A structure and the type B structure that can be interconverted when the transition metal is Ni. But when the transition metal is Pd or Pt, only the type B structure is observed and it is apparently not convertible to the type A structure. Details of the synthesis and characterization of $\{(DMF)_{10}Ln_2[Ni(CN)_4]_3\}_\infty$ in both type A (Ln = Sm, **1a**; Eu, **2a**) and type B (Ln = Sm, **1b**; Eu, **2b**) forms, $\{(DMF)_{10}Y_2[Pd(CN)_4]_3\}_\infty$, type B, and a new structural type of single-strand one-dimensional array, $\{(DMF)_{12}Ce_2[M(CN)_4]_3\}_\infty$ (M = Ni, Pd), designated as type C, are presented here.

Results and Discussion

A. Syntheses of $\{(DMF)_{10}Sm_2[Ni(CN)_4]_3\}_\infty$ (Type A and Type B), $\{(DMF)_{10}Eu_2[Ni(CN)_4]_3\}_\infty$ (Type A and Type B), and $\{(DMF)_{10}Y_2[Pd(CN)_4]_3\}_\infty$ (Type B). Synthesis of $\{(DMF)_{10}Sm_2[Ni(CN)_4]_3\}_\infty$ (type A) was discussed previously.[7a] $\{(DMF)_{10}Sm_2[Ni(CN)_4]_3\}_\infty$ (type A), **1a**, $\{(DMF)_{10}Sm_2[Ni(CN)_4]_3\}_\infty$ (type B), **1b**, $\{(DMF)_{10}Eu_2[Ni(CN)_4]_3\}_\infty$ (type A), **2a**, $\{(DMF)_{10}Eu_2[Ni(CN)_4]_3\}_\infty$ (type B), **2b**, and $\{(DMF)_{10}Y_2[Pd(CN)_4]_3\}_\infty$ (type B), **3**, were synthesized quantitatively according to eq 1.[7]

$$2LnCl_3 + 3K_2[M(CN)_4] \xrightarrow{DMF} \{(DMF)_{10}Ln_2[M(CN)_4]_3\}_\infty + 6KCl \quad (1)$$

1a (type A), **1b** (type B) (M = Ni, Ln = Sm)
2a (type A), **2b** (type B) (M = Ni, Ln = Eu)
3 (M = Pd, Ln = Y)

Complexes **2a** and **2b** were also synthesized, according to eq 2.

$$2EuCl_3 + 3NiCl_2 + 12KCN \xrightarrow{DMF} \{(DMF)_{10}Eu_2[Ni(CN)_4]_3\}_\infty + 12KCl \quad (2)$$

2a (type A), **2b** (type B)

Once the metathesis reactions were complete and KCl was removed, discrete single crystals were formed from concentrated DMF solutions. Crystals harvested shortly after they began to appear in the mother liquor were of the **1a** and **2a** type A complexes. They appear to be the kinetically favored form. However, they can be transformed to the apparently thermodynamically more stable type B form. When the crystals **1a** were allowed to remain in the saturated mother liquor for a period of ca. 10 days, they were converted to **1b**. Crystals of **2a** in saturated mother liquor were converted relatively rapidly to **2b** (less than 1 day). When **1b** and **2b** were dissolved in DMF, the initial crystals formed from these solutions were **1a** and **2a**, but upon standing in the saturated mother liquor they reverted to the **1b** and **2b** type. The type A and B crystals are distinguishable by their different crystalline habits as well as by X-ray crystallography and their solid state infrared spectra. Type A crystals are thin plates, while type B crystals are rhombuses.

For complex **3**, the crystals formed initially were type B. Extended periods of time in the saturated mother liquor did not change the structural type, and seeding a saturated solution of **3** with **1a** or **2a** still yielded only crystals of **3** in the type B form. Other Pd(II) and Pt(II) complexes $\{(DMF)_{10}Ln_2[M(CN)_4]_3\}_\infty$ (Ln, M = Sm, Pd; Eu, Pd; Yb, Pd; Yb, Pt)[7a] that crystallize initially as type B are also apparently not convertible to type A structures.

B. Molecular Structures of the One-Dimensional Arrays $\{(DMF)_{10}Ln_2[M(CN)_4]_3\}_\infty$ (Ln = Y, Sm, Eu; M = Ni, Pd). Crystal data for $\{(DMF)_{10}Sm_2[Ni(CN)_4]_3\}_\infty$ (type A), **1a**,$\{(DMF)_{10}Sm_2[Ni(CN)_4]_3\}_\infty$ (type B), **1b**, $\{(DMF)_{10}Eu_2[Ni(CN)_4]_3\}_\infty$ (type A), **2a**, $\{(DMF)_{10}Eu_2[Ni(CN)_4]_3\}_\infty$ (type B),

Table 1. Crystallographic Data for $\{(DMF)_{10}Sm_2[Ni(CN)_4]_3\}_\infty$ (Type A), **1a**, $\{(DMF)_{10}Sm_2[Ni(CN)_4]_3\}_\infty$ (Type B), **1b**, $\{(DMF)_{10}Eu_2[Ni(CN)_4]_3\}_\infty$ (Type A), **2a**, $\{(DMF)_{10}Eu_2[Ni(CN)_4]_3\}_\infty$ (Type B), **2b**, and $\{(DMF)_{10}Y_2[Pd(CN)_4]_3\}_\infty$ (Type B), **3**

	1a (type A)	**1b** (type B)	**2a** (type A)	**2b** (type B)	**3** (type B)
chemical formula	$C_{42}H_{70}O_{10}N_{22}Sm_2Ni_3$	$C_{42}H_{70}O_{10}N_{22}Sm_2Ni_3$	$C_{42}H_{70}O_{10}N_{22}Eu_2Ni_3$	$C_{42}H_{70}O_{10}N_{22}Eu_2Ni_3$	$C_{42}H_{70}O_{10}N_{22}Y_2Pd_3$
fw	1520.03	1520.03	1523.15	1523.15	1540.22
space group	$P\bar{1}$	$P\bar{1}$	$P\bar{1}$	$P\bar{1}$	$P\bar{1}$
a, Å	10.442(5)	9.129(2)	10.467(1)	9.128(1)	9.251(3)
b, Å	10.923(2)	11.286(6)	10.923(1)	11.271(1)	11.193(4)
c, Å	15.168(3)	16.276(7)	15.123(1)	16.227(6)	16.388(4)
α, deg	74.02(2)	81.40(4)	74.24(1)	81.36(2)	81.46(2)
β, deg	83.81(3)	77.41(3)	83.61(1)	77.43(2)	77.18(2)
γ, deg	82.91(4)	83.02(3)	83.13(1)	82.99(1)	83.24(3)
vol, Å^3	1645.6(9)	1611.3(12)	1646.4(2)	1604.0(6)	1629.9(8)
Z	1	1	1	1	1
ρ(calcd), Mg m^{-3}	1.534	1.567	1.536	1.577	1.569
T, ºC	−60	−60	−100	−60	−60
radiation (*λ*, Å)	Mo Kα (0.71073)	Mo Kα (0.71073)	MoKα (0.71073)	Mo Kα (0.71073)	Mo Kα (0.71073)
μ, mm^{-1}	2.661	2.718	2.781	2.855	2.636
R1[a] [$I > 2\sigma(I)$]	0.0352	0.0291	0.0295	0.0293	0.0347
wR2[b] (all data)	0.0945	0.0811	0.0772	0.0783	0.0954

[a] $R1 = \sum||F_o| - |F_c||/\sum|F_o|$. [b] $wR2 = \{\sum[w(F_o^2 - F_c^2)^2]/\sum[w(F_o^2)^2]\}^{1/2}$.

2b, and $\{(DMF)_{10}Y_2[Pd(CN)_4]_3\}_\infty$ (type B), **3**, are given in Table 1. Selected bond lengths and angles are listed in Table 2 for **1a** and **2a** and Table 3 for **1b**, **2b**, and **3**.

Complexes **1a** and **2a** adopt the structural type A, and complexes **1b**, **2b**, and **3** adopt the structural type B. These structures are isomorphous and isostructural with those type A and type B complexes reported earlier.[7] Crystal data for **1a** are presented in the Supporting Information of a previous publication.[7a] Since **1b**, **2b**, and **3** are isomorphous and isostructural, only **2b** is discussed in detail here and the structural details for **1b** and **3** are provided in the Supporting Information of this article.

The molecular structures of **2a** (type A) and **2b** (type B) are shown in Figures 1 and 2, respectively.

The average bond lengths for the Eu−O bond (2.376[10][8] Å for **2a** and 2.367[7][8] Å for **2b**) and for the Eu−N bond (2.513[6][8] Å for **2a** and 2.522[12][8] Å for **2b**) are comparable and are consistent with the sum of the Shannon crystal radii for Eu−O (2.416 Å) and Eu−N (2.526 Å).[9] The coordination geometries around Eu^{3+} in both **2a** and **2b** are a slightly distorted square antiprism very similar to that observed for other type A and type B structures.[7a] Figures of the coordination geometries of **2a** and **2b** are presented in the Supporting Information. The coordination geometries around Ni^{2+} in both **2a** and **2b** are approximately square planar.

C. Infrared Studies of Complexes of 1−3. In our earlier report on type A and type B complexes[7a] it was shown from solution infrared spectra, NMR spectra, and conductivity measurements in DMF that these types of complexes are dissociated in solution and most likely exist as ion pairs which retain some cyanide links between lanthanide and transition metal.

Infrared absorption frequencies for both Nujol mull and DMF solutions of the type A and type B complexes are reported in the Experimental Section. The infrared spectra of these complexes in the solid state (Nujol mull) and in DMF solutions are displayed in Figure 3, panels a and b, respectively.

The infrared spectral patterns for complexes **1a**, **1b**, **2a**, **2b**, and **3** in the solid state (Figure 3a) are consistent with those reported earlier for other type A and type B complexes,[7a] and spectral assignments (Experimental Section) are based upon earlier reported assignments.[7a,10] In the solid state infrared spectra, the absorption bands with the lowest wavenumbers for **1a** (2121 cm^{-1}), **1b** (2121 cm^{-1}), **2a** (2121 cm^{-1}), **2b** (2121 cm^{-1}), and **3** (2134 cm^{-1}) (Figure 3a) are assigned to the terminal cyanide stretching frequency. The remaining absorption bands are higher than the bands assigned to terminal cyanides; therefore, they are assigned to the bridging cyanide ligands. This assignment is consistent with the observation that typically bridging CN ligands have higher stretching frequencies than the terminal CN ligands.[10b] That the solid state (Figure 3a) and solution (Figure 3b) infrared spectra for the same complex display different patterns suggests that the solid state structure does not exist in the DMF solution. In the solution infrared spectra of **1a**, **1b**, **2a**, **2b**, and **3**, the lowest absorption band is assigned to the terminal cyanides. Several CN stretching bands at frequencies higher than that for terminal CN stretch indicate that the ion-paired complexes in solution contain cyanide bridges between the lanthanide and transition metal centers, consistent with results in our earlier report.[7a]

The infrared spectra of the type A and type B complexes in Nujol mull that contain Ni(II) are distinctly different and can be employed to distinguish between the two structural types.[7a] However, solution infrared spectra, shown in Figure 3b, obtained from the complexes of **1a**, **1b**, **2a**, and **2b** are identical, which is consistent with the observations that solutions of **1a**, **1b**, **2a**, and **2b** crystallize initially as the type A structures.

The Nujol mull infrared spectrum of **3**, which contains Pd(II), is similar to those of **1b** and **2b** because their structures are isomorphous and isostructural. However, its solution infrared spectrum differs from those of **1a**, **1b**, **2a**, and **2b**, which indicates that the ion-paired species in solution derived from **3** are structurally different from the ion-paired species derived from **1a**, **1b**, **2a**, and **2b**, though, in all cases, the infrared spectra indicate that some cyanide bridges exist in solution.

(8) Stout, G. H.; Jensen, L. H. In *X-ray Structure Determination*, 2nd ed.; Wiley: New York, 1989; pp 406−408. The standard deviation (σ_l) for the average Ln−N and Ln−O bond lengths is calculated according to the following equations from ref 8: $\langle l\rangle = \sum_m l_m/m$ and $\sigma_l = [\sum_m(l_m - \langle l\rangle)^2/m(m-1)]^{1/2}$ where $\langle l\rangle$ is the mean length, l_m is the length of the *m*th bond, and *m* is the number of bonds.

(9) Shannon, R. D. *Acta Crystallogr.* **1976**, *A32*, 751.

(10) (a) Kubas, G. J.; Jones, L. H. *Inorg. Chem.* **1974**, *13*, 2186. (b) Nakamoto, K. *Infrared and Raman Spectra of Inorganic and Coordination Compounds*, 4th ed.; Wiley and Sons: 1986 and references therein.

Table 2. Selected Bond Lengths (Å) and Angles (deg) for $\{(DMF)_{10}Sm_2[Ni(CN)_4]_3\}_\infty$ (Type A), **1a**, and $\{(DMF)_{10}Eu_2[Ni(CN)_4]_3\}_\infty$ (Type A), **2a**

1a (type A)		**2a** (type A)	
Bond Lengths			
Sm−O(3)	2.361(3)	Eu−O(2)	2.354(3)
Sm−O(2)	2.361(4)	Eu−O(3)	2.354(3)
Sm−O(1)	2.386(4)	Eu−O(1)	2.378(3)
Sm−O(5)	2.390(4)	Eu−O(5)	2.383(3)
Sm−O(4)	2.412(4)	Eu−O(4)	2.410(3)
Sm−N(11)	2.508(4)	Eu−N(11)	2.501(3)
Sm−N(12)#1[a]	2.518(4)	Eu−N(12)#1	2.510(3)
Sm−N(21)	2.540(4)	Eu−N(21)	2.529(3)
Ni(1)−C(11)	1.855(5)	Ni(1)−C(11)	1.860(4)
Ni(1)−C(12)	1.856(5)	Ni(1)−C(12)	1.866(4)
Ni(1)−C(13)	1.864(5)	Ni(1)−C(13)	1.869(4)
Ni(1)−C(14)	1.867(5)	Ni(1)−C(14)	1.872(4)
Ni(2)−C(21)	1.853(4)	Ni(2)−C(21)	1.863(3)
Ni(2)−C(22)	1.862(5)	Ni(2)−C(22)	1.866(4)
Angles			
O(3)−Sm−O(2)	143.93(13)	O(3)−Eu−O(2)	144.27(9)
O(3)−Sm−O(1)	109.67(14)	O(3)−Eu−O(1)	109.21(10)
O(2)−Sm−O(1)	80.15(15)	O(2)−Eu−O(1)	80.18(11)
O(3)−Sm−O(5)	73.06(14)	O(3)−Eu−O(5)	73.13(10)
O(2)−Sm−O(5)	140.44(14)	O(2)−Eu−O(5)	139.95(10)
O(1)−Sm−O(5)	70.57(15)	O(1)−Eu−O(5)	70.31(11)
O(3)−Sm−O(4)	80.18(14)	O(3)−Eu−O(4)	80.50(10)
O(2)−Sm−O(4)	73.03(14)	O(2)−Eu−O(4)	73.18(10)
O(1)−Sm−O(4)	142.70(14)	O(1)−Eu−O(4)	142.77(10)
O(5)−Sm−O(4)	144.15(14)	O(5)−Eu−O(4)	144.38(10)
O(3)−Sm−N(11)	142.00(13)	O(3)−Eu−N(11)	141.81(10)
O(2)−Sm−N(11)	72.79(14)	O(2)−Eu−N(11)	72.66(10)
O(1)−Sm−N(11)	80.15(14)	O(1)−Eu−N(11)	80.72(10)
O(5)−Sm−N(11)	76.40(15)	O(5)−Eu−N(11)	76.29(11)
O(4)−Sm−N(11)	114.76(15)	O(4)−Eu−N(11)	114.34(11)
O(3)−Sm−N(12)#1	76.14(13)	O(3)−Eu−N(12)#1	75.93(10)
O(2)−Sm−N(12)#1	117.30(14)	O(2)−Eu−N(12)#1	117.69(10)
O(1)−Sm−N(12)#1	143.12(13)	O(1)−Eu−N(12)#1	143.07(10)
O(5)−Sm−N(12)#1	77.06(15)	O(5)−Eu−N(12)#1	76.92(10)
O(4)−Sm−N(12)#1	73.64(13)	O(4)−Eu−N(12)#1	73.70(10)
N(11)−Sm−N(12)#1	75.42(13)	N(11)−Eu−N(12)#1	75.32(10)
O(3)−Sm−N(21)	73.52(13)	O(3)−Eu−N(21)	73.72(10)
O(2)−Sm−N(21)	76.95(13)	O(2)−Eu−N(21)	76.81(10)
O(1)−Sm−N(21)	72.70(13)	O(1)−Eu−N(21)	72.63(10)
O(5)−Sm−N(21)	116.87(15)	O(5)−Eu−N(21)	117.19(10)
O(4)−Sm−N(21)	76.30(14)	O(4)−Eu−N(21)	76.26(10)
N(11)−Sm−N(21)	142.16(13)	N(11)−Eu−N(21)	142.27(10)
N(12)#1−Sm−N(21)	140.19(13)	N(12)#1−Eu−N(21)	140.10(10)
C(11)−N(11)−Sm	165.5(4)	C(11)−N(11)−Eu1	65.1(3)
C(12)−N(12)−Sm#1	174.0(4)	C(12)−N(12)−Eu#1	173.7(3)
C(21)−N(21)−Sm	176.6(4)	C(21)−N(21)−Eu	176.3(3)
C(1)−O(1)−Sm	140.8(3)	C(1)−O(1)−Eu	140.3(2)
C(2)−O(2)−Sm	141.8(3)	C(2)−O(2)−Eu	141.3(2)
C(3)−O(3)−Sm	145.2(3)	C(3)−O(3)−Eu	145.0(3)
C(4)−O(4)−Sm	137.4(4)	C(4)−O(4)−Eu	136.9(3)
C(5)−O(5)−Sm	140.3(4)	C(5)−O(5)−Eu	139.8(3)
C(11)−Ni(1)−C(12)	91.16(19)	C(11)−Ni(1)−C(12)	91.01(15)
C(11)−Ni(1)−C(13)	174.2(2)	C(11)−Ni(1)−C(13)	174.28(17)
C(11)−Ni(1)−C(14)	89.5(2)	C(11)−Ni(1)−C(14)	89.42(16)
C(12)−Ni(1)−C(13)	89.5(2)	C(12)−Ni(1)−C(13)	89.58(15)
C(12)−Ni(1)−C(14)	177.0(2)	C(12)−Ni(1)−C(14)	177.38(18)
C(13)−Ni(1)−C(14)	90.2(2)	C(13)−Ni(1)−C(14)	90.25(16)
C(21)−Ni(2)−C(22)	89.00(19)	C(21)−Ni(2)−C(22)	88.92(15)
N(11)−C(11)−Ni(1)	175.2(5)	N(11)−C(11)−Ni(1)	174.7(3)
N(12)−C(12)−Ni(1)	177.8(4)	N(12)−C(12)−Ni(1)	178.1(3)
N(13)−C(13)−Ni(1)	176.4(6)	N(13)−C(13)−Ni(1)	177.2(4)
N(14)−C(14)−Ni(1)	178.7(6)	N(14)−C(14)−Ni(1)	178.7(4)
N(21)−C(21)−Ni(2)	178.3(4)	N(21)−C(21)−Ni(2)	178.1(3)
N(22)−C(22)−Ni(2)	177.7(5)	N(22)−C(22)−Ni(2)	177.9(3)

[a] Symmetry transformations used to generate equivalent atoms: (#1) $-x+1, -y, -z+1$; (#2) $-x, -y, -z$.

Table 3. Selected Bond Lengths (Å) and Angles (deg) for $\{(DMF)_{10}Sm_2[Ni(CN)_4]_3\}_\infty$ (Type B), **1b**, $\{(DMF)_{10}Eu_2[Ni(CN)_4]_3\}_\infty$ (Type B), **2b**, and $\{(DMF)_{10}Y_2[Ni(CN)_4]_3\}_\infty$ (Type B), **3**

	1b (Ln = Sm, M = Ni)	**2b** (Ln = Eu, M = Ni)	**3** (Ln = Y, M = Pd)
Bond Lengths			
Ln−O(1)	2.358(4)	2.340(4)	2.288(4)
Ln−O(2)	2.399(3)	2.381(3)	2.337(4)
Ln−O(3)	2.390(3)	2.378(3)	2.324(4)
Ln−O(4)	2.383(3)	2.372(3)	2.308(4)
Ln−O(5)	2.383(4)	2.366(4)	2.319(4)
Ln−N(11)	2.544(4)	2.532(4)	2.480(5)
Ln−N(12)#1[a]	2.548(4)	2.536(4)	2.476(4)
Ln−N(21)	2.509(4)	2.497(4)	2.449(5)
M(1)−C(11)	1.863(4)	1.864(5)	1.983(6)
M(1)−C(12)	1.869(4)	1.865(5)	1.994(6)
M(1)−C(13)	1.864(5)	1.862(5)	1.989(6)
M(1)−C(14)	1.870(5)	1.871(5)	2.002(6)
M(2)−C(21)	1.860(5)	1.859(5)	1.992(6)
M(2)−C(22)	1.866(5)	1.870(5)	1.984(6)
Angles			
O(1)−Ln−O(5)	73.5(2)	73.1(2)	72.5(2)
O(1)−Ln−O(4)	141.79(14)	141.90(14)	141.87(16)
O(5)−Ln−O(4)	79.53(19)	80.12(19)	80.9(2)
O(1)−Ln−O(3)	143.61(15)	143.61(16)	142.79(15)
O(5)−Ln−O(3)	140.25(17)	140.53(17)	141.86(19)
O(4)−Ln−O(3)	71.87(15)	71.82(15)	72.48(17)
O(1)−Ln−O(2)	81.55(16)	81.82(16)	80.66(16)
O(5)−Ln−O(2)	145.01(15)	144.97(15)	144.98(16)
O(4)−Ln−O(2)	107.83(14)	107.51(15)	109.26(17)
O(3)−Ln−O(2)	71.89(14)	71.81(14)	71.37(15)
O(1)−Ln−N(21)	114.01(15)	113.81(16)	114.87(17)
O(5)−Ln−N(21)	72.17(14)	72.25(14)	72.85(17)
O(4)−Ln−N(21)	81.80(13)	81.99(13)	81.31(16)
O(3)−Ln−N(21)	76.83(14)	76.75(14)	76.50(17)
O(2)−Ln−N(21)	141.90(13)	141.81(13)	140.60(15)
O(1)−Ln−N(11)	71.55(13)	71.48(13)	70.71(15)
O(5)−Ln−N(11)	117.56(17)	117.04(17)	114.18(18)
O(4)−Ln−N(11)	146.37(14)	146.33(14)	146.87(16)
O(3)−Ln−N(11)	77.92(14)	77.92(14)	78.91(16)
O(2)−Ln−N(11)	75.49(13)	75.73(13)	75.97(14)
N(21)−Ln−N(11)	77.19(13)	76.97(13)	76.00(15)
O(1)−Ln−N(12)#1	75.18(13)	75.35(14)	75.92(15)
O(5)−Ln−N(12)#1	77.66(14)	77.70(14)	78.51(15)
O(4)−Ln−N(12)#1	72.94(13)	72.81(13)	72.34(15)
O(3)−Ln−N(12)#1	117.75(13)	117.85(13)	116.99(15)
O(2)−Ln−N(12)#1	72.40(13)	72.50(13)	73.39(14)
N(21)−Ln−N(12)#1	143.57(12)	143.53(12)	143.64(15)
N(11)−Ln−N(12)#1	136.38(12)	136.59(12)	137.57(15)
C(11)−N(11)−Ln	152.4(3)	152.8(3)	153.2(4)
C(12)−N(12)−Ln#2	169.5(3)	169.8(3)	170.0(4)
C(21)−N(21)−Ln	172.4(4)	172.8(4)	174.4(4)
C(1)−O(1)−Ln	143.8(4)	143.9(4)	146.8(4)
C(2)−O(2)−Ln	143.5(4)	143.6(4)	141.0(4)
C(3)−O(3)−Ln	136.4(5)	136.8(5)	135.3(5)
C(4)−O(4)−Ln	135.8(5)	135.9(5)	139.7(6)
C(5)−O(5)−Ln	152.6(6)	152.1(6)	154.4(6)
C(11)−M(1)−C(12)	92.00(18)	92.13(18)	93.0(2)
C(11)−M(1)−C(13)	178.8(2)	178.7(2)	178.5(2)
C(11)−M(1)−C(14)	89.92(19)	89.78(19)	89.2(2)
C(12)−M(1)−C(13)	88.87(19)	88.8(2)	87.8(2)
C(12)−M(1)−C(14)	178.06(19)	178.1(2)	177.7(2)
C(13)−M(1)−C(14)	89.2(2)	89.2(2)	90.1(2)
C(21)−M(2)−C(22)	89.8(2)	89.9(2)	89.7(2)
N(11)−C(11)−M(1)	176.8(4)	176.5(4)	176.4(4)
N(12)−C(12)−M(1)	176.6(4)	176.3(4)	175.4(4)
N(13)−C(13)−M(1)	178.0(6)	178.1(6)	177.1(6)
N(14)−C(14)−M(1)	178.8(5)	178.6(5)	178.1(5)
N(21)−C(21)−M(2)	179.1(4)	178.8(4)	178.1(5)
N(22)−C(22)−M(2)	178.9(6)	178.8(6)	178.5(6)

[a] Symmetry transformations used to generate equivalent atoms: (#1) $x-1, y, z$; (#2) $x+1, y, z$.

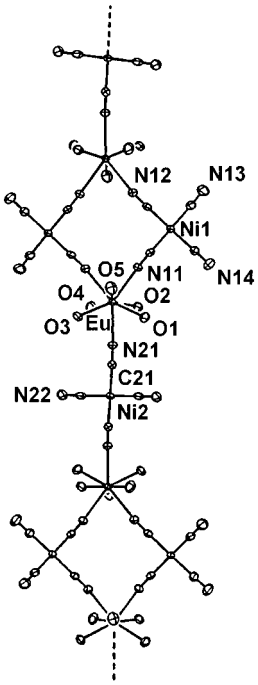

Figure 1. Molecular structure (50% thermal ellipsoids) of a portion of the one-dimensional array **2a** (only the oxygen atoms of the DMF are shown for clarity).

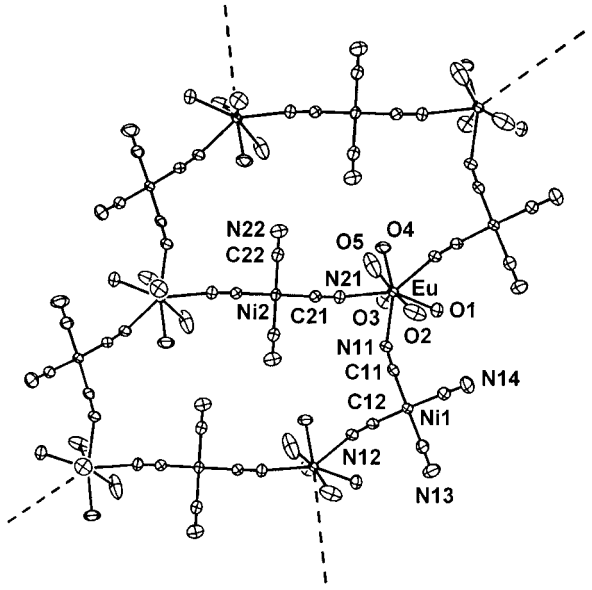

Figure 2. Molecular structure (50% thermal ellipsoids) of a portion of the one-dimensional array **2b** (only the oxygen atoms of the DMF are shown for clarity).

D. Syntheses of Type C Complexes. The one-dimensional arrays, $\{(DMF)_{12}Ce_2[M(CN)_4]_3\}_\infty$ (M = Ni, **4**; Pd, **5**), were prepared according to eq 3 and eq 4, respectively.

$$2CeCl_3 + 3NiCl_2 + 12KCN \xrightarrow{DMF} \underset{\mathbf{4}}{\{(DMF)_{12}Ce_2[Ni(CN)_4]_3\}_\infty} + 12KCl \quad (3)$$

$$2CeCl_3 + 3K_2[Pd(CN)_4] \xrightarrow{DMF} \underset{\mathbf{5}}{\{(DMF)_{12}Ce_2[Pd(CN)_4]_3\}_\infty} + 6KCl \quad (4)$$

Once the metathesis reactions were complete and KCl was removed, discrete single crystals of **4** and **5** were formed from concentrated DMF solutions. As shown below in section E, the structures of **4** and **5** are similar to the type A structure, but unlike type A complexes they could not be converted to a crystal structure related to the type B structure. Crystals of **4** and **5** allowed to remain in the saturated mother liquor for ca. 3 months were unchanged. Isolated crystals of **4** and **5** tend to readily lose DMF, and reasonable analyses could not be obtained. However, three crystals of each type of complex were verified by single-crystal X-ray crystallography.

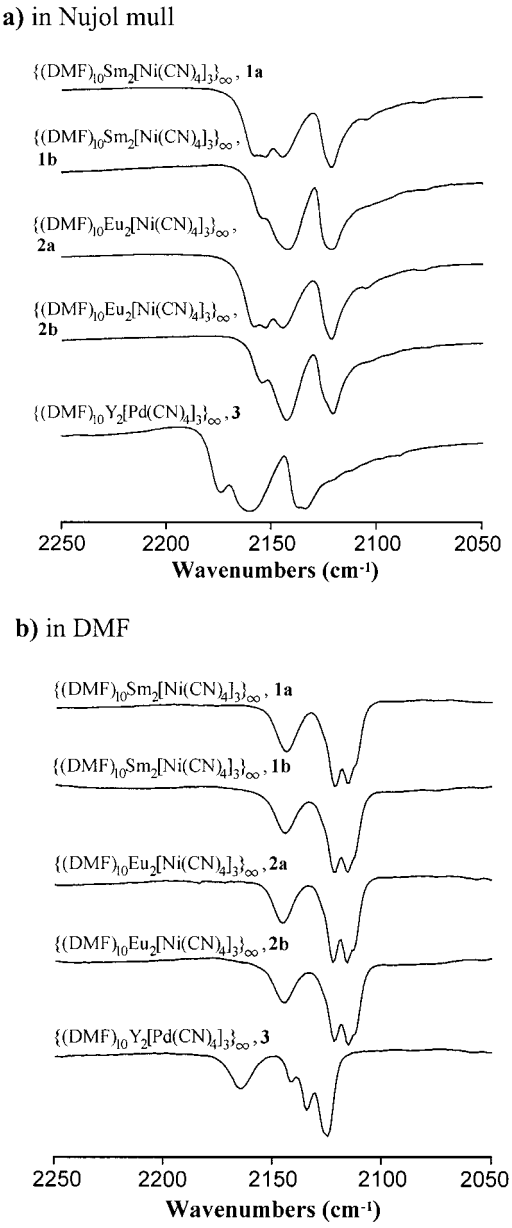

Figure 3. (a) Solid state (Nujol mull) and (b) solution (DMF) infrared spectra of **1a**, **1b**, **2a**, **2b**, and **3**.

E. Molecular Structures of the One-Dimensional Arrays $\{(DMF)_{12}Ce_2[M(CN)_4]_3\}_\infty$ (M = Ni, 4; Pd, 5). Single-crystal X-ray analyses show the structures of **4** (Figure 4) and **5** to be isomorphous and isostructural. Crystallographic data and selected bond distances and angles are listed in Tables 4 and 5. Molecular structures of **4** and **5** are designated as type C. The type C structure contains a "diamond"-shaped Ce_2M_2 (M = Ni, Pd) metal core like that of type A,[7a] formed by two $[M(CN)_4]^{2-}$ (M = Ni, Pd) anions that bridge two Ce^{3+} centers in a cis fashion. These "diamond"-shaped metal cores are linked by

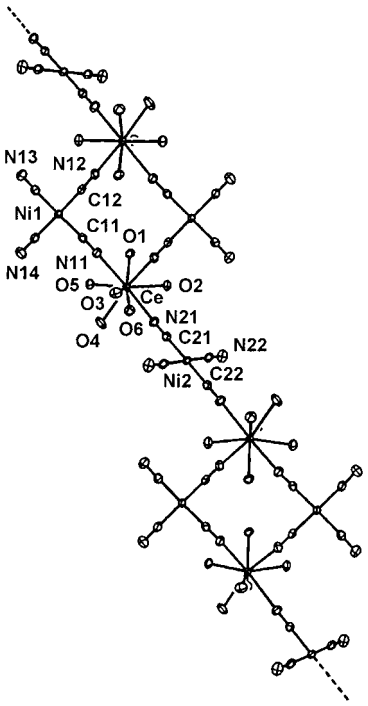

Figure 4. Molecular structure (50% thermal ellipsoids) of a portion of the one-dimensional array **4** (only the oxygen atoms of the DMF are shown for clarity).

Table 4. Crystallographic Data for $\{(DMF)_{12}Ce_2[Ni(CN)_4]_3\}_\infty$, **4**, and $\{(DMF)_{12}Ce_2[Pd(CN)_4]_3\}_\infty$, **5**

	4 (type C)	**5** (type C)
formula	$C_{48}H_{84}N_{24}O_{12}Ce_2Ni_3$	$C_{48}H_{84}N_{24}O_{12}Ce_2Pd_3$
fw	1645.76	1788.83
space group	$P\bar{1}$	$P\bar{1}$
a, Å	11.279(1)	11.388(3)
b, Å	12.504(1)	12.614(5)
c, Å	13.887(1)	13.965(4)
α, deg	98.68(1)	97.67(3)
β, deg	108.85(1)	109.01(2)
γ, deg	101.75(1)	101.93(2)
vol, Å^3	1764.6(2)	1811.5(10)
Z	1	1
ρ(calcd), Mg m^{-3}	1.549	1.640
T, °C	−80	−60
radiation (*λ*, Å)	Mo Kα (0.71073)	Mo Kα (0.71073)
μ, mm^{-1}	2.118	2.028
R1[a] [$I > 2\sigma(I)$]	0.0199	0.0250
wR2[b] (all data)	0.0473	0.0666

[a] $R1 = \sum||F_o| - |F_c||/\sum|F_o|$. [b] $wR2 = \{\sum[w(F_o^2 - F_c^2)^2]/\sum[w(F_o^2)^2]\}^{1/2}$.

$[M(CN)_4]^{2-}$ anions that are bound to the Ce^{3+} centers through the cyanide bridges in a trans fashion (Figure 4) to generate zigzag one-dimensional arrays (Figure 4), in contrast to the straight-chain one-dimensional linear array type A structure (Figure 1).

In addition to the zigzag structure, another major difference between type C and type A structures is that the Ce^{3+} ion is 9-coordinate (Figure 5), a monocapped square antiprismatic geometry, rather than the 8-coordinate square antiprismatic arrangement in the type A structure. In the coordination geometry around Ce^{3+}, the arrangement of the CN ligands determines the zigzag character of the array and also accommodates the diamond-shaped core.

The average Ce−O bond lengths are 2.520[10][8] and 2.520[10][8] Å for **4** and **5**, while the average Ce−N bond lengths are 2.645[3][8] and 2.642[3][8] Å for **4** and **5**. These distances are

Table 5. Selected Bond Lengths (Å) and Angles (deg) for $\{(DMF)_{12}Ce_2[Ni(CN)_4]_3\}_\infty$ (Type C), **4**, and $\{(DMF)_{12}Ce_2[Pd(CN)_4]_3\}_\infty$ (Type C), **5**

4 (type C)		**5** (type C)	
	Bond Lengths		
Ce−O(1)	2.4806(14)	Ce−O(1)	2.478(3)
Ce−O(4)	2.4835(16)	Ce−O(4)	2.481(3)
Ce−O(3)	2.5059(15)	Ce−O(3)	2.499(3)
Ce−O(2)	2.5310(14)	Ce−O(2)	2.516(3)
Ce−O(6)	2.5589(14)	Ce−O(5)	2.554(3)
Ce−O(5)	2.5626(15)	Ce−O(6)	2.560(3)
Ce−N(11)	2.6486(18)	Ce−N(11)	2.641(4)
Ce−N(12)#1[a]	2.6338(18)	Ce−N(12)#1	2.647(4)
Ce−N(21)	2.6513(17)	Ce−N(21)	2.639(4)
Ni(1)−C(11)	1.866(2)	Pd(1)−C(11)	1.993(5)
Ni(1)−C(12)	1.870(2)	Pd(1)−C(12)	1.995(5)
Ni(1)−C(13)	1.867(2)	Pd(1)−C(13)	1.984(5)
Ni(1)−C(14)	1.872(2)	Pd(1)−C(14)	1.986(5)
Ni(2)−C(21)	1.870(2)	Pd(2)−C(21)	1.988(5)
Ni(2)−C(22)	1.876(2)	Pd(2)−C(22)	1.991(5)
	Angles		
O(1)−Ce−O(4)	136.98(5)	O(1)−Ce−O(4)	137.36(11)
O(1)−Ce−O(3)	136.26(5)	O(1)−Ce−O(3)	135.95(11)
O(4)−Ce−O(3)	71.11(6)	O(4)−Ce−O(3)	70.60(13)
O(1)−Ce−O(2)	69.34(5)	O(1)−Ce−O(2)	69.64(10)
O(4)−Ce−O(2)	126.43(6)	O(4)−Ce−O(2)	127.19(12)
O(3)−Ce−O(2)	127.10(5)	O(3)−Ce−O(2)	126.58(11)
O(1)−Ce−O(6)	70.46(5)	O(1)−Ce−O(6)	70.56(10)
O(4)−Ce−O(6)	67.90(5)	O(4)−Ce−O(6)	67.94(11)
O(3)−Ce−O(6)	111.14(5)	O(3)−Ce−O(6)	111.30(11)
O(2)−Ce−O(6)	121.73(5)	O(2)−Ce−O(6)	122.09(11)
O(1)−Ce−O(5)	82.65(5)	O(1)−Ce−O(5)	83.69(11)
O(4)−Ce−O(5)	71.80(6)	O(4)−Ce−O(5)	71.93(13)
O(3)−Ce−O(5)	139.92(5)	O(3)−Ce−O(5)	139.27(11)
O(2)−Ce−O(5)	67.42(5)	O(2)−Ce−O(5)	67.95(11)
O(6)−Ce−O(5)	67.17(5)	O(6)−Ce−O(5)	67.44(10)
O(1)−Ce−N(12)#1	79.00(5)	O(1)−Ce−N(12)#1	79.35(11)
O(4)−Ce−N(12)#1	141.93(6)	O(4)−Ce−N(12)#1	140.88(12)
O(3)−Ce−N(12)#1	72.40(6)	O(3)−Ce−N(12)#1	71.79(12)
O(2)−Ce−N(12)#1	70.38(5)	O(2)−Ce−N(12)#1	70.22(11)
O(6)−Ce−N(12)#1	137.56(5)	O(6)−Ce−N(12)#1	138.00(10)
O(5)−Ce−N(12)#1	137.61(5)	O(5)−Ce−N(12)#1	138.07(11)
O(1)−Ce−N(11)	72.59(5)	O(1)−Ce−N(11)	72.08(11)
O(4)−Ce−N(11)	101.03(6)	O(4)−Ce−N(11)	100.82(13)
O(3)−Ce−N(11)	68.54(5)	O(3)−Ce−N(11)	68.75(11)
O(2)−Ce−N(11)	132.29(5)	O(2)−Ce−N(11)	131.81(11)
O(6)−Ce−N(11)	68.18(5)	O(6)−Ce−N(11)	68.42(11)
O(5)−Ce−N(11)	133.99(5)	O(5)−Ce−N(11)	134.57(11)
O(1)−Ce−N(21)	138.71(5)	O(1)−Ce−N(21)	138.83(10)
O(4)−Ce−N(21)	73.28(6)	O(4)−Ce−N(21)	73.50(12)
O(3)−Ce−N(21)	71.13(5)	O(3)−Ce−N(21)	71.00(11)
O(2)−Ce−N(21)	69.46(5)	O(2)−Ce−N(21)	69.29(11)
O(5)−Ce−N(21)	84.15(5)	O(5)−Ce−N(21)	83.61(11)
O(6)−Ce−N(21)	137.10(5)	O(6)−Ce−N(21)	137.14(11)
N(11)−Ce−N(12)#1	75.10(6)	N(11)−Ce−N(12)#1	74.93(11)
N(11)−Ce−N(21)	138.77(6)	N(11)−Ce−N(21)	138.76(12)
N(21)−Ce−N(12)#1	85.04(6)	N(21)−Ce−N(12)#1	84.52(12)
C(11)−N(11)−Ce1	68.34(16)	C(11)−N(11)−Ce1	67.4(3)
C(12)−N(12)−Ce#1	164.15(17)	C(12)−N(12)−Ce#1	163.5(3)
C(21)−N(21)−Ce1	75.77(17)	C(21)−N(21)−Ce1	74.5(4)
C(1)−O(1)−Ce1	31.37(14)	C(1)−O(1)−Ce1	32.9(3)
C(2)−O(2)−Ce1	31.91(14)	C(2)−O(2)−Ce1	33.3(3)
C(3)−O(3)−Ce1	36.11(14)	C(3)−O(3)−Ce1	37.4(3)
C(4)−O(4)−Ce1	43.25(15)	C(4)−O(4)−Ce1	44.5(3)
C(5)−O(5)−Ce1	19.75(14)	C(5)−O(5)−Ce1	20.6(3)
C(6)−O(6)−Ce1	48.24(15)	C(6)−O(6)−Ce1	48.4(3)
C(11)−Ni(1)−C(12)	91.65(9)	C(11)−Pd(1)−C(12)	91.43(16)
C(11)−Ni(1)−C(13)	172.79(10)	C(11)−Pd(1)−C(13)	175.01(18)
C(11)−Ni(1)−C(14)	89.58(9)	C(11)−Pd(1)−C(14)	88.84(17)
C(12)−Ni(1)−C(13)	88.87(9)	C(12)−Pd(1)−C(13)	89.31(17)
C(12)−Ni(1)−C(14)	173.09(9)	C(12)−Pd(1)−C(14)	174.93(17)
C(13)−Ni(1)−C(14)	90.77(9)	C(13)−Pd(1)−C(14)	90.85(18)
C(21)−Ni(2)−C(22)	91.58(9)	C(21)−Pd(2)−C(22)	88.13(17)
N(11)−C(11)−Ni(1)	174.05(19)	N(11)−C(11)−Pd(1)	173.9(4)
N(12)−C(12)−Ni(1)	174.21(19)	N(12)−C(12)−Pd(1)	173.2(4)
N(13)−C(13)−Ni(1)	176.4(2)	N(13)−C(13)−Pd(1)	177.1(5)
N(14)−C(14)−Ni(1)	178.2(2)	N(14)−C(14)−Pd(1)	177.4(4)
N(21)−C(21)−Ni(2)	178.57(19)	N(21)−C(21)−Pd(2)	178.5(4)
N(22)−C(22)−Ni(2)	177.67(19)	N(22)−C(22)−Pd(2)	177.9(4)

[a] Symmetry transformations used to generate equivalent atoms: (#1) $-x, -y + 1, -z + 1$; (#2) $-x, -y + 2, -z + 2$.

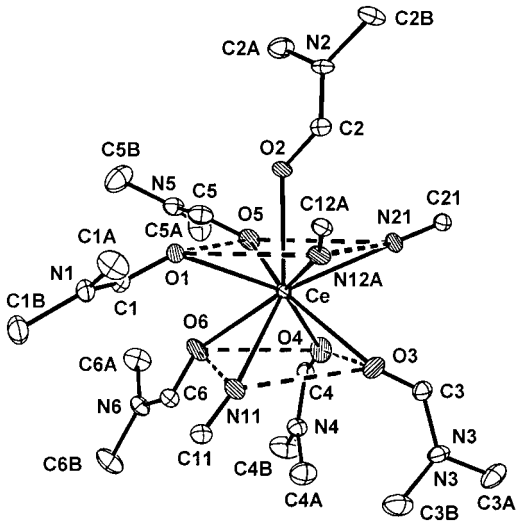

Figure 5. Coordination geometry around the Ce^{3+} in **4**.

comparable to the sum of the Shannon crystal radii for Ce−O (2.546 Å) and Ce−N (2.656 Å).[9] According to the Shannon crystal radii, the size difference between 9-coordinated Ce^{3+} (1.336 Å)[9] and 8-coordinated Eu^{3+} (1.206 Å)[9] is 0.13 Å. The observed average Ce−O and Ce−N bond lengths are 0.144 and 0.132 Å longer than Eu−O and Eu−N bond lengths in complex **2a**, respectively. The slightly greater bond length difference between the sum of the Shannon crystal radii and the observed average bond lengths for Ce−O and Eu−O bonds may come from the steric effect around the lanthanide centers as shown in Figure 6. The distances between the adjacent vertexes in the mono-capped square base in the type C complex, **4**, range from 3.255(2) to 3.572(2) Å (Figure 6a), much larger than those (between 2.840(4) and 3.062(5) Å) (Figure 6b) in the type A complex, **2a**. On the bottom square base, the distances between the adjacent vertexes are very similar in both **4** (2.817(2)−2.920(2) Å) (Figure 6a) and **2a** (2.7414(4)−2.933(4) Å) (Figure 6b). The extra capped DMF molecule has forced the capped square base to open up to reduce the steric effect so that it can coordinate to the Ce^{3+} center.

The coordination geometries around the nickel and palladium atoms in **4** and **5** are approximately square planar as in complexes with type A and B structures.

F. Infrared Studies of Complexes of 4 and 5. Infrared absorption frequencies for both Nujol mull and DMF solutions of the type C complexes, **4** and **5**, are reported in the Experimental Section.

For type C complexes **4** and **5** (Figure 7), the infrared spectra in solution depend on the transition metal. The solution infrared spectrum of **4**, which contains Ni(II), displays a pattern similar to that for the type A complexes **1a** and **2a** (Figures 7 and 3, Experimental Section). However, for complex **5** which contains Pd(II), its infrared spectrum in solution is similar to that for type B complexes, such as **3** (Figures 7 and 3, Experimental Section). The solution infrared spectra of **4** and **5** differ from their solid state spectra, but the solution spectra indicate that the ion-paired species retain some cyanide bridges.

G. Discussion

1. Type A and Type B Structures. This work, coupled with other results from this laboratory,[7] shows that the cyanide-bridged lanthanide−transition metal complexes with DMF ligands that contain Ni(II) and Ln(III) (Ln = Sm, Eu) can crystallize as extended single-strand arrays (type A) or extended

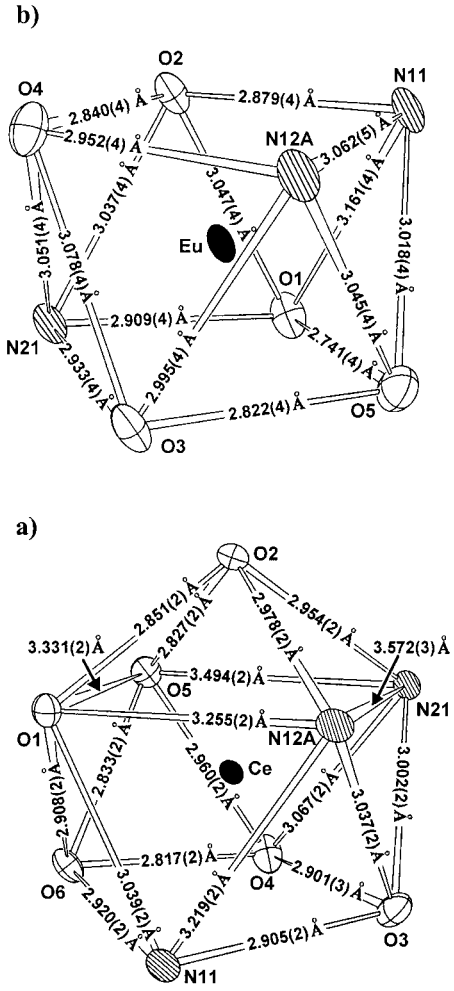

Figure 6. Schematic presentation of distances between the adjacent vertexes of the polyhedrons showing the coordination geometries of (a) Ce^{3+} (type C) and (b) Eu^{3+} (type A).

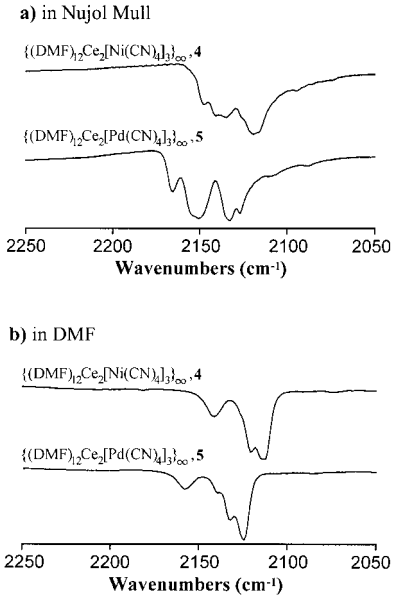

Figure 7. (a) Solid state (Nujol mull) and (b) solution (DMF) infrared spectra of **4** and **5**.

double-strand arrays (type B). The structures are interconvertible. The type A crystals are the initial crystalline product that deposits from solution and are considered to be the kinetically

favored crystalline form, but extended time in the mother liquor causes their conversion to type B crystals. The rate of conversion in the mother liquor appears to depend upon the lanthanide, being rapid for the Eu−Ni combination but considerably slower for the Sm−Ni combination. When the type B crystals are dissolved in DMF, type A crystals are the first to form but convert to type B upon residing in the mother liquor for an extended period of time. These results are consistent with infrared spectra of solutions which are prepared from type A and type B crystals that contain Ni(II). These solutions produce identical infrared spectra, indicating the presence of identical or very similar species in solution, which results in initial crystallization of type A crystals irrespective of whether the solution was obtained from type A or type B crystals. While the solution infrared spectra of the Ni(II) complexes are identical, the (Nujol mull) infrared spectra of the type A and type B solids are significantly different.

On the other hand, complexes that contain Pd(II) or Pt(II)[7a] in combination with Ln(III) (Ln = Y, Sm, Eu, Yb) appear to give type B crystals directly. Their (Nujol mull) infrared spectra are consistent with the Nujol mull infrared spectra observed for the type B complexes that contain Ni(II), but their solution infrared spectra differ from the solution infrared spectra obtained from the type A and type B solids that contain Ni(II).

Earlier, conductivity studies[7a] showed that complexes that contain Ni(II), type A or B, and complexes that contain Pd(II) or Pt(II), type B, are partially ionized in DMF solution and have similar conductivities at similar concentrations irrespective of whether the solution was derived from type A or type B complexes that contain Ni(II). This ionization probably occurs through rupture of some of the lanthanide−nitrogen bonds in the cyanide bridges because the transition metal−carbon bond in the $M(CN)_4$ (M = Ni, Pd, Pt) unit is stronger than the lanthanide−nitrogen bond. But the infrared spectra show that some of the lanthanide−cyanide−transition metal bridges remain. This is also true for the infrared spectra of **3** and other type B complexes that contain Pd(II) or Ni(II) in DMF.[7a] While DMF solutions of **1a**, **1b**, **2a**, and **2b** are essentially identical, their spectra differ markedly from the infrared spectrum of **3** in DMF solution, which contains Pd(II). The determining factor as to whether an interconvertible type A or type B structure forms or the nonconvertible type B structure forms appears to be the nature of the ionic species in solution, which based upon the infrared spectra appear to be structurally different for the complexes that contain Pd(II) or Pt(II) compared to those complexes that contain Ni(II). At this point we cannot account for this distinction. Other than the fact that ionic species exist in solution and they are oligomeric, the sizes and distribution of oligomer sizes are unknown and not accessible.

There is no obvious clue as to why the type B structure appears to be the thermodynamically favored form, except that the type B complexes are slightly more dense (ca. 1.5%) than the type A complexes. There appear to be no unusual close contacts or differences in bond distances and angles that would suggest that one structural type should be favored over the other.

2. New Structural Type, Type C. Complexes **4** and **5** contain 9-coordinate Ce^{3+} and possess a new type of structure, designated type C. The solution infrared spectra of type C complexes have features similar to those for type A and type B complexes. When nickel is the transition metal, the solution infrared spectrum resembles that of the convertible type A complexes. On the other hand, when palladium is the transition metal, the solution infrared spectrum has features similar to those of the nonconvertible type B complexes. Thus nickel and palladium appear to have similar roles in determining the infrared spectra of type C in solutions as in type A and type B complexes.

Experimental Section

General Data. All manipulations were carried out on a standard high vacuum line or in a drybox under an atmosphere of dry, pure N_2. The purification of DMF (Baker) and the activation of Linde brand molecular sieves (4 Å) are described in a previous publication.[7a]

Fourier transform infrared (FTIR) spectra were recorded on a Mattson Polaris Fourier transform spectrometer with 2 cm^{-1} resolution. Samples were prepared as solutions or Nujol mulls. Nujol samples were analyzed as films placed between KBr plates in an airtight sample holder. Solution spectra were obtained using airtight Perkin-Elmer cells with 0.1 mm Teflon spacers between KBr or NaCl windows. All IR samples were prepared in the drybox. Elemental analyses of materials were performed by Oneida Research Services, Inc., Whitesboro, NY, or by Galbraith Laboratories, Inc., Knoxville, TN.

$K_2[Ni(CN)_4]\cdot H_2O$ (Strem) was dried under vacuum at 150 °C for 16 h and stored in the drybox. $K_2[Pd(CN)_4]\cdot 3H_2O$ (Aldrich) was dried under vacuum at 100 °C for 12 h and then at 200 °C for 0.5 h and stored in the drybox. Anhydrous YCl_3 (Strem), $CeCl_3$ (Strem), $SmCl_3$ (Strem), $EuCl_3$ (Strem), $YbCl_3$ (Strem), $NiCl_2$ (Aldrich), and KCN (Aldrich) were used as received. The preparation of $\{(DMF)_{10}Sm_2[Ni(CN)_4]_3\}_\infty$, **1a**, with type A structure was reported earlier.[7a]

Preparation of $\{(DMF)_{10}Sm_2[Ni(CN)_4]_3\}_\infty$ (Type B), 1b. $SmCl_3$ (200 mg, 0.799 mmol) and 281.5 mg (1.168 mmol) of $K_2[Ni(CN)_4]$ in a 2:3 ratio were stirred in DMF (ca. 15 mL) at room temperature over 5 days. The resulting solution was filtered, leaving a white precipitate (KCl) and a yellow filtrate. The DMF was pumped away until a viscous oil remained. Within 24−48 h, the yellow thin-plate-like crystals of $\{(DMF)_{10}Sm_2[Ni(CN)_4]_3\}_\infty$, **1a**, with structural type A were formed, and they were left in the flask with mother liquor for 10 days. These yellow thin-plate-like crystals, **1a** (type A), were slowly converted into rhombohedral crystals, **1b** (type B). Yield: nearly quantitative. The crystals were pumped on under vacuum for 12−14 h, resulting in the loss of 1 DMF molecule per empirical unit as determined by elemental analysis. Anal. Calcd for $C_{39}H_{63}N_{21}O_9Sm_2Ni_3$: C, 32.38; H, 4.39; N, 20.33. Found: C, 31.67; H, 4.16; N, 20.20. IR (Nujol mull of crystals, ν_{CN}, cm^{-1}): 2155 (m, sh), 2143 (s), 2121 (s). IR (DMF solution, ν_{CN}, cm^{-1}): 2144 (m), 2122 (s), 2116 (s), 2112 (s, sh).

Preparation of $\{(DMF)_{10}Eu_2[Ni(CN)_4]_3\}_\infty$ (Type A), 2a. Two methods were employed to prepare this complex.

Method 1. $EuCl_3$ (100 mg, 0.387 mmol) and 140 mg (0.584 mmol) of $K_2[Ni(CN)_4]$ in a 2:3 ratio were stirred in DMF (ca. 15 mL) at room temperature over 5 days. The resulting solution was filtered, leaving a white precipitate (KCl) and a yellow filtrate. DMF was pumped away until a viscous oil remained. Yellow thin-plate-like X-ray quality type A crystals formed after 24 h at room temperature. Yield: nearly quantitative.

Method 2. $EuCl_3$ (103.3 mg, 0.4 mmol), 77.8 mg (0.6 mmol) of $NiCl_2$, and 156.3 mg (2.4 mmol) of KCN in a 2:3:12 ratio were stirred in DMF (ca. 20 mL) at room temperature over 7 days. The resulting solution was filtered, leaving a white precipitate (KCl) and a yellow filtrate. The DMF was pumped away until a viscous oil remained. Yellow thin-plate-like type A X-ray quality crystals formed after 24 h at room temperature. Yield: nearly quantitative.

Samples for elemental analysis were obtained by drying crystals under vacuum for 12−14 h. One DMF molecule per empirical unit was lost after drying as determined by the elemental analysis. Anal. Calcd for $C_{39}H_{67}N_{21}O_9Ni_3Eu_2$: C, 32.30; H, 4.38; N, 20.28. Found: C, 32.31; H, 4.27; N, 20.00. IR (Nujol mull of crystals, ν_{CN}, cm^{-1}): 2158 (s), 2153 (s), 2144 (s), 2121 (vs). IR (DMF solution, ν_{CN}, cm^{-1}): 2145 (m), 2122 (s), 2116 (s), 2112 (s, sh).

Preparation of $\{(DMF)_{10}Eu_2[Ni(CN)_4]_3\}_\infty$ (Type B), 2b. After the yellow thin-plate-like crystals of $\{(DMF)_{10}Eu_2[Ni(CN)_4]_3\}_\infty$, **2a**, of structural type A were formed, they were left in the flask with mother liquor for 1 day. These crystals slowly transformed into yellow crystals of structural type B. Yield: nearly quantitative.

Elemental analysis for the solids obtained from drying of the crystals under vacuum for 12−14 h: One DMF molecule per empirical unit was lost after drying as determined by elemental analysis. Anal. Calcd for $C_{39}H_{67}N_{21}O_9Ni_3Eu_2$: C, 32.30; H, 4.38; N, 20.28. Found: C, 32.81; H, 4.29; N, 20.07. IR (Nujol mull of crystals, ν_{CN}, cm^{-1}): 2155 (m), 2143 (s), 2121 (s). IR (DMF solution, ν_{CN}, cm^{-1}): 2145 (m), 2122 (s), 2116 (s), 2112 (s, sh).

Preparation of $\{(DMF)_{10}Y_2[Pd(CN)_4]_3\}_\infty$ (Type B), 3. YCl_3 (117.2 mg, 0.60 mmol) and 258.9 mg (0.90 mmol) of $K_2[Pd(CN)_4]$ in a 2:3 ratio were stirred in DMF (ca. 15 mL) at room temperature over 5 days. The resulting solution was filtered, leaving a white precipitate (KCl) and a colorless filtrate. The DMF was pumped away until a viscous oil remained. X-ray quality crystals were obtained after 24 h at room temperature. Yield: nearly quantitative. Elemental analysis for the solids obtained from drying the crystals under vacuum for 12−14 h: Anal. Calcd for $C_{42}H_{70}N_{22}O_{10}Y_2Pd_3$: C, 32.82; H, 4.59; N, 20.05. Found: C, 32.43; H, 4.34; N, 19.81. IR (Nujol mull of crystals, ν_{CN}, cm^{-1}): 2174 (m), 2161 (s), 2138 (s), 2134 (s). IR (DMF solution, ν_{CN}, cm^{-1}): 2166 (m), 2142 (m), 2135 (s), 2125 (vs).

Preparation of $\{(DMF)_{12}Ce_2[Ni(CN)_4]_3\}_\infty$ (Type C), 4. $CeCl_3$ (250 mg, 1.01 mmol), 197 mg (1.52 mmol) of $NiCl_2$, and 396 mg (6.08 mmol) of KCN were stirred in ca. 20 mL of dry DMF for 6 days at room temperature. The reaction mixture was filtered, leaving a white precipitate on the frit (KCl) and a yellow filtrate. DMF was pumped away until a viscous oil remained. Within 24 h at room temperature, thin-plate-like yellow X-ray quality crystals of $\{(DMF)_{12}Ce_2[Ni(CN)_4]_3\}_\infty$ formed. IR (Nujol mull of crystals, ν_{CN}, cm^{-1}): 2148 (s), 2141 (s), 2135 (s), 2119 (vs). IR (DMF solution, ν_{CN}, cm^{-1}): 2142 (m), 2121 (s), 2115 (s), 2113 (sh, s).

Preparation of $\{(DMF)_{12}Ce_2[Pd(CN)_4]_3\}_\infty$ (Type C), 5. $CeCl_3$ (359.1 mg, 1.46 mmol) and 628.7 mg (2.19 mmol) of $K_2[Pd(CN)_4]$ were dissolved in ca. 20 mL of dry DMF. After 5 days of stirring at room temperature, the reaction mixture was filtered, leaving a white precipitate on the frit (KCl) and a colorless filtrate. The DMF was pumped away until a viscous oil remained. X-ray quality crystals of $\{(DMF)_{12}Ce_2[Pd(CN)_4]_3\}_\infty$ formed after 48 h at room temperature. IR (Nujol mull of crystals, ν_{CN}, cm^{-1}): 2166 (m), 2155 (s, sh), 2150 (s), 2133 (s), 2127 (s). IR (DMF solution, ν_{CN}, cm^{-1}): 2160 (m), 2141 (m), 2133 (s), 2125 (vs).

X-ray Structure Determination. Single-crystal X-ray diffraction data were collected either on an Enraf-Nonius CAD4 diffractometer using graphite-monochromated Mo Kα radiation or on an Enraf-Nonius KappaCCD diffraction system with graphite-monochromated Mo Kα radiation.

When the Enraf-Nonius CAD4 diffractometer was used, suitable single crystals were mounted and sealed inside glass capillaries of 0.3 or 0.5 mm diameter under N_2. Unit cell parameters were obtained by a least-squares refinement of the angular settings from 25 reflections, well distributed in reciprocal space and lying in the 2θ range of 24−30°. The diffraction data were corrected for Lorentz and polarization effects and empirical absorption (empirically from ψ-scan data).

When the Enraf-Nonius KappaCCD diffraction system was employed, the crystal was mounted on the tip of a glass fiber coated with Parabar. Unit cell parameters were obtained by indexing the peaks in the first 10 frames and refined employing the whole data set. All frames were integrated and corrected for Lorentz and polarization effects using DENZO.[11] The empirical absorption correction was applied with SORTAV.[12]

The structures were solved by direct methods and refined using SHELXTL (difference electron density calculations, full least-squares refinements).[13] Two types of rotationally disordered DMF molecules in **1b**, **2b**, and **3** were observed identical to those in the type B complexes reported earlier.[7a]

Acknowledgment. This work was supported by the National Science Foundation through Grant CHE 99-01115.

Supporting Information Available: Listings of crystallographic data, positional parameters, anisotropic thermal parameters, bond distances, and bond angles for all complexes, the figures of coordination geometries of Eu^{3+} in **2a** and **2b**, and the discussion of these coordination geometries. This material is available free of charge via the Internet at http://pubs.acs.org.

IC001143P

(11) Otwinowsky, Z.; Minor, W. Processing of X-ray Diffraction Data Collected in Oscillation Mode. In *Methods in Enzymology, Vol. 276: Macromolecular Crystallogrphy, part A*; Carter, C. W., Jr., Sweet, R. M., Eds.; Academic Press: New York, 1997; pp 307−326.
(12) Blessing, R. H. *Acta Crystallogr.* **1995**, *A51*, 33.
(13) SHELXTL (version 5.10), Bruker Analytical X-ray Systems, 1997.